Available online at www.sciencedirect.com
ScienceDirect
International Journal of Thermal Sciences 46 (2007) 93–103
International Journal of Thermal Sciences
www.elsevier.com/locate/ijts

Analysis of an air cooled ammonia–water vertical tubular absorber

José Fernández-Seara *, Francisco J. Uhía, Jaime Sieres

Área de Máquinas y Motores Térmicos, Escuela Técnica Superior de Ingenieros Industriales, Campus Lagoas-Marcosende, N°9, 36310 Vigo, Spain

Received 24 December 2004; received in revised form 27 October 2005; accepted 29 March 2006

Available online 5 June 2006

Abstract

This paper presents a detailed analysis of an ammonia–water vertical tubular absorber cooled by air. The absorption process takes place co-currently upward inside the tubes. The tubes are externally finned with continuous plate fins and the tube rows are arranged staggered in the direction of the air flow. The air is forced over the tube bank and circulates between the plain fins in cross flow with the ammonia–water mixture. The analysis has been carried out by means of a mathematical model developed on the basis of mass and energy balances and heat and mass transfer equations. The model takes into account separately the churn, slug and bubbly flow patterns experimentally forecasted in this type of absorption processes inside vertical tubes and considers the simultaneous heat and mass transfer processes in both liquid and vapour phases, as well as heat transfer to the cooling air. The model has been implemented in a computer program. Results based on a representative design and nominal operating conditions of an absorber for a small capacity ammonia–water absorption refrigeration system are shown. A parametric analysis was realised to investigate the influence of the design parameters and operating conditions on the absorber performance. The noteworthy results that have effect on practical design of the absorber are presented and commented.
© 2006 Elsevier Masson SAS. All rights reserved.

Keywords: Absorber; Ammonia–water; Air cooled; Absorption; Refrigeration

1. Introduction

Absorption systems are heat powered, therefore they can contribute to the recovery of exhaust heat at low temperatures that is now being rejected into the atmosphere from different types of processes. They can also contribute to more efficient energy utilisation when they are integrated with other technologies such as cogeneration systems [1,2]. Moreover, they are an interesting option to obtain solar cooling for air conditioning purposes when coupled with thermal solar plants thus promoting the use of renewable energies [3]. Therefore, the interest on developing more efficient absorption systems in order to spread out their use is high.

The initial investment required in absorption systems constitutes the main obstacle for the extension of their use. If water is used as cooling medium for the absorber, then a cooling tower will be required and the initial cost of the installation and its complexity will increase. This is significant for small power machines where the investment in the cooling tower together with the complexity added to the installation constitute an important drawback for broadening the use of these systems. Therefore, the development of air-cooled absorbers and their application in absorption machines constitutes an outstanding challenge since it would avoid the use of the cooling tower and would reduce the initial cost of the installation.

There are studies that consider the use of air cooled absorbers in water–LiBr absorption systems from a theoretical and experimental view points [4–6]. However, the use of air cooled absorbers in water–LiBr systems increases the risk of crystallisation due to the absorption temperatures being higher using air than using water as cooling medium. Moreover, the absorption temperature is also above the ambient air temperature and therefore it can reach high values in hot climates or summer time. The risk of crystallisation increases in simple effect systems and therefore in the cheapest and more demanded machines. Thus, the air-cooled absorbers in water–LiBr systems are mainly proposed for double effect machines. However, the authors have not found any water–LiBr ma-

* Corresponding author. Tel.: +34 986 812605; fax: +34 986 811995.
E-mail addresses: jseara@uvigo.es (J. Fernández-Seara), jsieres@uvigo.es (J. Sieres).

1290-0729/$ – see front matter © 2006 Elsevier Masson SAS. All rights reserved.
doi:10.1016/j.ijthermalsci.2006.03.005

Nomenclature

A	transfer area	m^2
a_{esp}	specific interfacial area	$m^2\,m^{-3}$
c	heat transfer correction factor	
c_p	specific heat	$J\,kg^{-1}\,K^{-1}$
$\tilde{c}_p$	partial mass specific heat	$J\,kg^{-1}\,K^{-1}$
d	tube diameter	m
F	mass transfer coefficient	$kmol\,m^{-2}\,s^{-1}$
$F(R, P)$	correction factor for the logarithmic mean temperature difference	
h	specific enthalpy	$J\,kg^{-1}$
$\tilde{h}$	partial enthalpy	$J\,kg^{-1}$
i	element incremental number	
j	row incremental number	
k_w	tube wall thermal conductivity	$W\,m^{-1}\,K^{-1}$
$\overline{M}$	molecular weight	$kg\,kmol^{-1}$
$\dot{M}$	mass flow	$kg\,s^{-1}$
$\dot{m}$	mass flux	$kg\,m^{-2}\,s^{-1}$
n	number of discrete elements	
n_r	number of tube rows	
$\dot{n}$	molar flux	$kmol\,m^{-2}\,s^{-1}$
r_i	interfacial radius	m
S_d	diagonal tube spacing	m
S_f	fin spacing	m
S_l	longitudinal tube spacing	m
S_t	transversal tube spacing	m
T	temperature	K
t_f	fin thickness	m
U_o	overall heat transfer coefficient	$W\,m^{-2}\,K^{-1}$
V_{Lf}	mean velocity in the film	$m\,s^{-1}$
x	ammonia mass concentration	$(kg\ NH_3)\,kg^{-1}$
$\bar{x}$	ammonia molar concentration	$(kmol\ NH_3)\,kmol^{-1}$
z	ratio of ammonia to the total molar flux	

Greek symbols

α	heat transfer coefficient	$W\,m^{-2}\,K^{-1}$
ε_v	void fraction	
φ	heat flux	$W\,m^{-2}$
η	overall outer surface efficiency	
η_f	fin efficiency	

Subscripts

b	bulk
c	coolant
ci	coolant inlet to tube rows
co	coolant outlet from tube rows
f	fin
i	interface
L	liquid
Lb	bulk liquid
Lsp	liquid single-phase
v	vapour
w	wall
wi	inner wall
wo	outer wall

chine commercially available equipped with an air cooled absorber.

Ammonia–water systems do not present any limiting factor such as crystallisation for the use of high absorption and condensation temperatures. However, it should be borne in mind that it leads to a system performance reduction [7]. Air cooled absorbers and condensers are used in ammonia–water commercially available machines of small cooling capacities [8,9]. These machines are designed to produce chilled water for air conditioning systems. New models are also used as heat pumps to produce hot water. The main advantage of these systems lies in avoiding the use of the cooling tower; however these commercial machines present the inconvenience of being gas-fired, so they are unable to operate with any other kind of heat source which requires the use of a secondary thermal fluid such as hot water or vapour. The air cooled absorbers employed in ammonia–water commercial machines are conventional finned tube heat exchangers. The tubes are arranged horizontally and the air is forced by a fan. The weak solution from the generator is expanded and mixed with the vapour from the evaporator in a preabsorber or premixer recipient. Then, the liquid–vapour mixture is forced to circulate through the absorber tubes by the pump of the system located at the absorber outlet. The two phase flow is cooled by air and the ammonia vapour is absorbed into the liquid solution.

In this paper an ammonia–water vertical tubular absorber cooled by air is analysed. This type of absorbers is recommended for ammonia–water absorption systems because of the high heat and mass transfer coefficients encountered. However, at present, neither air cooled nor water cooled vertical tubular absorbers have been incorporated into the commercial machines and remain into the research state. Ref. [10] reports a detailed analysis of the heat and mass transfer processes during the absorption of ammonia into water in a co-current vertical tubular absorber of the shell and tubes type using water as cooling medium. In the analysis of the absorption process inside the tubes the churn, slug and bubbly flow patterns are considered separately as well as the simultaneous heat and mass transfer processes in the liquid and vapour phases and the heat transfer to the cooling medium. The analysis has been carried out by developing a differential mathematical model based on mass and energy balances and heat and mass transfer equations using local heat and mass transfer coefficients. This reference also includes a literature review of the theoretical and experimental research works related to this type of absorbers; therefore it is not repeated here.

The analysis presented in this paper is based on the general mathematical model initially developed for a water cooled absorber reported in Ref. [10]. However, further modifications have been introduced to take into account the new absorber con-

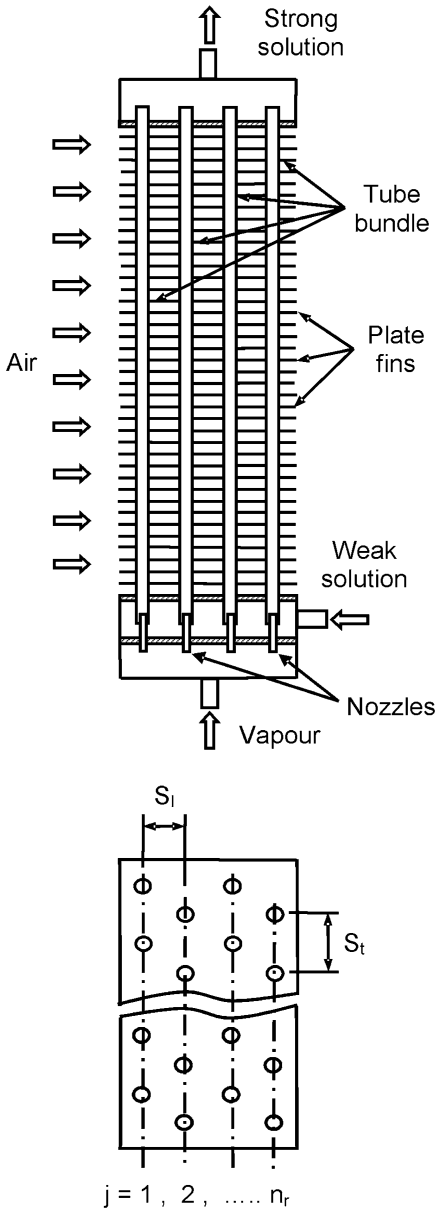

Fig. 1. Schematic diagram of the air cooled vertical tubular absorber.

figuration and geometry and the use of air as cooling medium. In this paper the model is summarised and the changes introduced are detailed. The results shown herein are focused on the particularities introduced by the air cooling of the absorber and those results that do not bring a new contribution to the results shown in Ref. [10] are avoided for the sake of brevity.

2. System description

A schematic diagram of the air cooled vertical tubular absorber considered in the analysis is shown in Fig. 1. The absorber consists of a vertical bundle of tubes. The tube rows are arranged staggered in the direction of the air flow and the tubes are finned externally with continuous plate fins. The geometrical parameters that characterise the tubes and the fins as well as the tubes arrangement in the bundle are depicted in Figs. 1 and 2. The ammonia vapour and the weak ammonia–water liquid solution are distributed at the bottom of the absorber and circulate co-currently upwards within the tubes. The vapour enters at the bottom of the absorber and is ducted in the tubes through small diameter nozzles. The liquid phase (weak solution) is also introduced at the bottom of the absorber, going into the tubes through the free area between tubes and nozzles. The absorption process progresses as the vapour and liquid contact inside the tubes. The liquid solution obtained (strong solution) is removed at the top of the absorber. The air is forced over the tube bundle and circulates between the plate fins in cross flow with the ammonia–water mixture which passes through the tubes. The air contacts the tube rows of the bundle consecutively, as can be seen from Fig. 1.

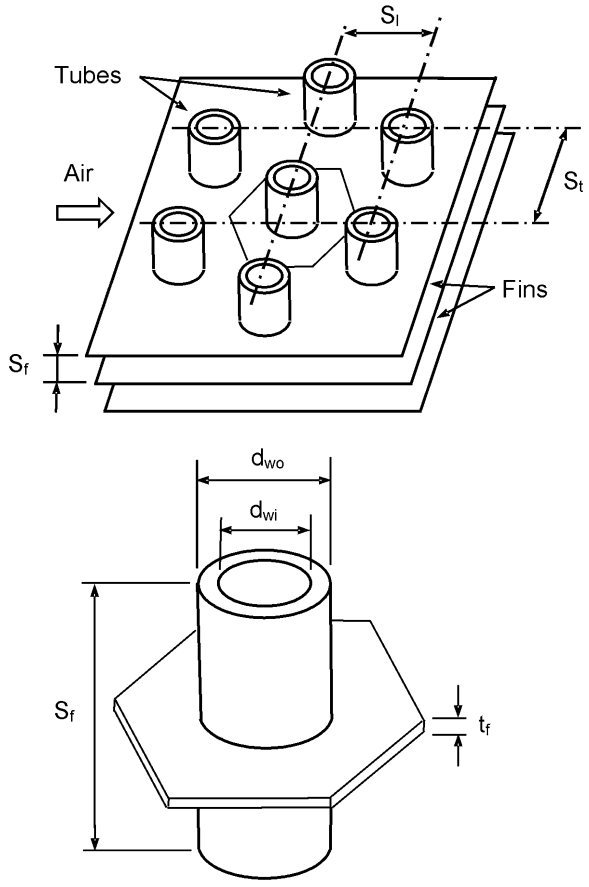

Fig. 2. Incremental element.

3. Mathematical model

The distributed modelling method has been applied to build the mathematical model. The absorber tubes are segmented into a number of incremental elements equal to the number of fins per tube. Each discrete element is composed of the corresponding portions of tube and fin. The discrete element considered in the analysis is represented in Fig. 2. The mathematical model has been developed on the basis of mass and energy balances and heat and mass transfer equations applied to each discrete tube-fin element. The model takes into account separately the churn, slug and bubbly flow patterns and considers the simul-

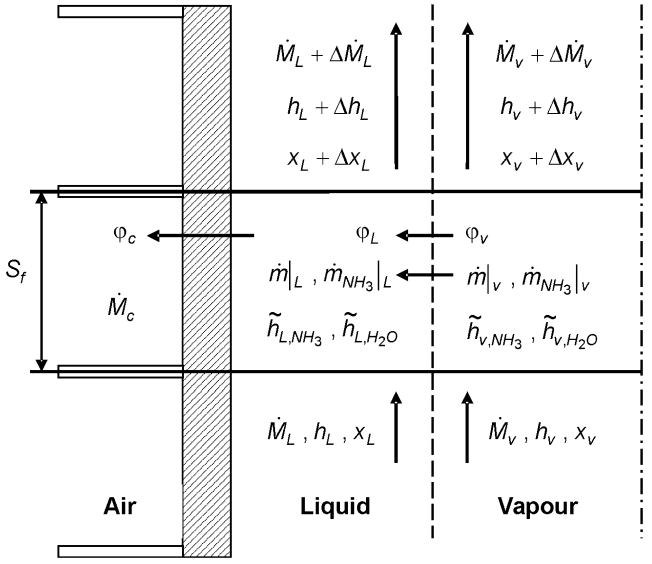

Fig. 3. Incremental control volume.

taneous heat and mass transfer processes in both liquid and vapour phases and the heat transfer to the cooling air through the finned tube. In order to analyse the absorption process, mass, concentration and energy balances are considered, as well as mass and heat transfer equations have been applied to each discrete element. The heat transfer to the cooling air is computed taking into account the bare tube and the fin surface areas and the fin efficiency. The control volume considered in the analysis where the model equations are applied is shown in Fig. 3.

The following assumptions have been made to develop the model.

(1) The absorption process is in steady state and the absorber pressure is constant.
(2) The two-film and the Lewis and Whitman theory [11] of non-interfacial resistance are applied, i.e., the interface concentrations of vapour and liquid are the equilibrium concentrations at the interface temperature.
(3) The heat and mass transfer areas between liquid and vapour phases are equal.
(4) In each discrete element, the coolant, liquid and vapour properties are assumed to be constant.
(5) Bubble coalescence and break-up are not considered.
(6) There is no direct heat transfer between the vapour and the cooling air.
(7) The heat transfer by conduction in the direction of the tubes and nearby fins is neglected.
(8) There is no contact heat-resistance between the fin and the tube.
(9) The air-facing velocity to the absorber is in a homogeneous distribution.

3.1. Mass transfer equations

Mass transfer between the vapour and the liquid phases results from the combined contribution of molecular diffusion and a bulk transport of material through the interface [10–15]. The molar flux of ammonia from the bulk vapour to the interface and from the interface to the bulk liquid is obtained from Eqs. (1) and (2), respectively, where mass transfer is defined to be positive from the vapour to the interface and from the interface to the liquid.

$$\dot{n}_{\mathrm{NH_3}}\big|_v = F_v \cdot z \cdot \mathrm{Ln}\left(\frac{z - \bar{x}_{vi}}{z - \bar{x}_{vb}}\right) \tag{1}$$

$$\dot{n}_{\mathrm{NH_3}}\big|_L = F_{Li} \cdot z \cdot \mathrm{Ln}\left(\frac{z - \bar{x}_{Lb}}{z - \bar{x}_{Li}}\right) \tag{2}$$

In Eqs. (1) and (2), z is the ratio of the molar flux of ammonia to the total molar flux $\dot{n}$ (ammonia and water molar fluxes).

The mass continuity requirement at the interface yields Eq. (3).

$$\dot{n}_{\mathrm{NH_3}}\big|_L = \dot{n}_{\mathrm{NH_3}}\big|_v = \dot{n} \cdot z \tag{3}$$

The ammonia and total mass fluxes are obtained from the corresponding molar fluxes taking into account the components' molecular weight, according to Eqs. (4) and (5).

$$\dot{m}_{\mathrm{NH_3}} = \dot{n}_{\mathrm{NH_3}} \cdot \overline{M}_{\mathrm{NH_3}} \tag{4}$$

$$\dot{m} = \dot{n}_{\mathrm{NH_3}} \cdot \overline{M}_{\mathrm{NH_3}} + \dot{n} \cdot (1 - z) \cdot \overline{M}_{\mathrm{H_2O}} \tag{5}$$

3.2. Heat transfer equations

Mass and heat transfer processes take place simultaneously in the vapour and liquid phases. The sensible heats transferred from the bulk vapour to the interface and from the interface to the bulk liquid are given by Eqs. (6) and (7), respectively.

$$\varphi_v = \alpha_v \cdot \frac{c_v}{1 - e^{-c_v}} \cdot (T_{vb} - T_i) \tag{6}$$

$$\varphi_L = \alpha_{Li} \cdot \frac{c_L}{1 - e^{-c_L}} \cdot (T_i - T_{Lb}) \tag{7}$$

with c being

$$c = \frac{\dot{m}_{\mathrm{NH_3}} \cdot \tilde{c}_{p,\mathrm{NH_3}} + \dot{m}_{\mathrm{H_2O}} \cdot \tilde{c}_{p,\mathrm{H_2O}}}{\alpha} \tag{8}$$

The energy balance at the liquid–vapour interface provides Eq. (9), according to the control volume shown in Fig. 3.

$$\varphi_L = \varphi_v + \dot{m}_{\mathrm{NH_3}} \cdot \Delta\tilde{h}_{\mathrm{NH_3}} + \dot{m}_{\mathrm{H_2O}} \cdot \Delta\tilde{h}_{\mathrm{H_2O}} \tag{9}$$

where $\Delta\tilde{h}$ is the components' difference of vapour and liquid partial enthalpies at the interface conditions.

The heat flux transferred from the bulk liquid to the cooling air is given by Eq. (10).

$$\varphi_c = U_o \cdot \Delta T_{LM} \cdot F(R, P) \tag{10}$$

where, U_o is the overall heat transfer coefficient referred to the outer finned tube surface, ΔT_{LM} is the logarithmic mean temperature difference defined in Eq. (11) and $F(R, P)$ is the correction factor for the logarithmic mean temperature difference which in this case is equal to 1 as corresponds to a cross flow with the hot fluid at constant temperature.

$$\Delta T_{LM} = \frac{(T_{Lb} - T_{ci}) - (T_{Lb} - T_{co})}{\mathrm{Ln}\left[\frac{T_{Lb} - T_{ci}}{T_{Lb} - T_{co}}\right]} \tag{11}$$

The overall heat transfer coefficient is obtained from Eq. (12).

$$\frac{1}{U_o} = \frac{\Delta A_c}{\alpha_{Lw} \cdot \Delta A_L} + \frac{\Delta A_c}{2 \cdot \pi \cdot k_w \cdot S_f} \cdot \mathrm{Ln}\left(\frac{d_{wo}}{d_{wi}}\right) + \frac{1}{\alpha_c \cdot \eta} \quad (12)$$

being α_{Lw} the heat transfer coefficient between the liquid phase and the inner tube wall, α_c the heat transfer coefficient between the outer surface and the cooling air, ΔA_L the element inner tube area which is obtained from Eq. (13), ΔA_c the element total outer surface area given by Eq. (14) and η is the overall outer surface efficiency given by Eq. (15)

$$\Delta A_L = \pi \cdot d_{wi} \cdot S_f \quad (13)$$

$$\Delta A_c = \pi \cdot d_{wo} \cdot (S_f - t_f) + 2 \cdot \left(S_t \cdot S_l - \frac{\pi \cdot d_{wo}^2}{4}\right) \quad (14)$$

$$\eta = 1 - \frac{\Delta A_f}{\Delta A_c} \cdot (1 - \eta_f) \quad (15)$$

In Eq. (15), η_f is the fin efficiency and ΔA_f is the element fin area. The fin efficiency (η_f) is obtained from the empirical solution given by Schmidt [16] for hexagonal fins (see Fig. 2) taking into account the modifications proposed by Hong and Webb [17] and Perrotin and Clodic [18] in order to improve its accuracy. The element fin area is given by Eq. (16).

$$\Delta A_f = 2 \cdot \left(S_t \cdot S_l - \frac{\pi \cdot d_{wo}^2}{4}\right) \quad (16)$$

3.3. Mass and energy balances

The mass, concentration and energy balances over the control volume shown in Fig. 3 yield Eqs. (17), (18) and (19), respectively.

$$\Delta \dot{M}_v = -\Delta \dot{M}_L \quad (17)$$

$$\Delta(\dot{M}_v \cdot x_v) = -\Delta(\dot{M}_L \cdot x_L) \quad (18)$$

$$\Delta(\dot{M}_v \cdot h_v) = -\Delta(\dot{M}_L \cdot h_L) - \varphi_c \cdot \Delta A_c \quad (19)$$

An analysis of the bulk vapour phase leads to Eqs. (20), (21) and (22).

$$\Delta \dot{M}_v = -\dot{m} \cdot \Delta A_i \quad (20)$$

$$\Delta(\dot{M}_v \cdot x_v) = -\dot{m}_{\mathrm{NH_3}} \cdot \Delta A_i \quad (21)$$

$$\Delta(\dot{M}_v \cdot h_v) = -(\dot{m}_{\mathrm{NH_3}} \cdot \tilde{h}_{v,\mathrm{NH_3}} + \dot{m}_{\mathrm{H_2O}} \cdot \tilde{h}_{v,\mathrm{H_2O}} + \varphi_v) \cdot \Delta A_i \quad (22)$$

The heat and mass transfer area between the liquid and vapour phases ΔA_i is given in Eq. (23), where a_{esp} is the specific interfacial area.

$$\Delta A_i = a_{esp} \cdot \frac{\pi \cdot d_{wi}^2}{4} \cdot S_f \quad (23)$$

Eqs. (1)–(23) constitute the mathematical model of the absorber.

3.4. Flow patterns and flow parameters

In vertical tubular absorbers with co-currently upward flow inside the tubes, churn, slug and bubbly flow patterns are present, according to the experimental observations of Infante Ferreira [19]. Churn flow takes place at the entrance, slug flow at the intermediate stage and bubbly flow at the end part of the absorption process. The characteristics of each flow pattern are reviewed in Ref. [10]. Therefore, herein only the criteria and correlations implemented in the model to calculate the characteristic flow parameters are summarised.

The churn flow pattern is studied under the annular flow model, according to Ueda [20]. The interfacial radius r_i and the mean velocity in the liquid film, V_{Lf}, are calculated iteratively from the Hikita and Ishimi [21] relations. The slug flow pattern is characterised by the vapour phase rising as Taylor bubbles, according to [22] separated by slugs of liquid. It is assumed that the Taylor bubbles consist of a half sphere nose followed by a cylindrical body and they are surrounded by a thin liquid film. The interfacial radius r_i of the Taylor bubble and the mean velocity in the liquid film, V_{Lf} are calculated by means of an iterative procedure detailed in Ref. [10]. The bubbly flow pattern is characterised by isolated spherical bubbles rising co-currently with the liquid [23] and arises at the end part of the absorption process. The initial bubble size and frequency are calculated iteratively as indicated in Ref. [10] taking into account the slug flow pattern and the Taylor bubble behaviour at the initial conditions, since the churn flow pattern is considered only an entrance effect. The two-phase flow void fraction is obtained from Nicklin et al. [24] in churn and slug flows and from Zuber and Findlay [25] in bubbly flow. The specific interfacial area in churn and in slug flow is calculated as the surface area of the bubble per unit liquid–vapour volume [13]. In bubbly flow the correlation proposed by Hikita et al. [26] is used.

3.5. Mass and heat transfer coefficients

Mass and heat transfer coefficients between the vapour-interface and liquid-interface are obtained according to the Refs. [27–35] cited in Table 1. The heat transfer coefficient between the liquid and the inner tube wall in churn flow is considered to be equal to the heat transfer coefficient between the

Table 1
Mass and heat transfer coefficients between vapour–liquid phases

	Flow pattern	Mass transfer	Heat transfer
Vapour to interface	Churn flow	Chilton Colburn analogy [27]	Gnielinski [28]
	Slug flow	Chilton Colburn analogy [27]	Gnielinski [28]
	Bubble flow	Clift et al. [29]	Chilton Colburn analogy [27]
Liquid to interface	Churn flow	Chilton Colburn analogy [27]	Film wise condensation [30–32]
	Slug flow	Lamourelle and Sandall [33]	Film wise condensation [30–32]
	Bubble flow	Hughmark [34]	Deckwer [35]

liquid phase and the liquid–vapour interface. In slug and bubbly flows it is calculated taking into account the heat transfer coefficient between the liquid-interface and the single-phase heat transfer coefficient obtained from Gnielinski [28] for turbulent flow and from Kays and Crawford [36] for laminar flow, using the formula proposed by Keizer [37] (Eq. (24)). The heat transfer coefficient between the outer finned surface of tubes and the cooling air is obtained from the Colburn factor evaluated from McQuiston and Parker [38].

$$\alpha_{Lw} = \varepsilon_v \cdot \alpha_{Li} + (1 - \varepsilon_v) \cdot \alpha_{Lsp} \tag{24}$$

4. Solution method

The absorber is composed of a vertical tube bundle arranged in rows staggered in the air flow direction (see Fig. 1). The weak solution and the vapour enter at the bottom of the absorber and are distributed among the tubes. Therefore, the liquid and vapour conditions are known at the inlet of each tube. The absorption process progresses as the vapour and liquid contact inside the tubes, therefore the conditions of the internal flow change from the bottom to the top in each tube. The cooling air is forced over the tube bundle and circulates between the plane fins without mixing in the tubes direction. The air passes in cross flow with the ammonia–water mixture which circulates from the bottom to the top inside the tubes. Moreover, the air circulating between the fins contacts consecutively the different tube rows and heats up when passing over each row. Therefore, the air temperature will vary along the tubes length and in the air flow direction and it will be different at the inlet of each element in each tube row. Then, the evolution of the absorption process inside the tubes will be different among the tubes in the different rows. However, the absorption process in the tubes in the same row will be equal since the inlet air conditions are the same for all tubes.

In the analysis each tube has been divided in a finite number of elements n, with an incremental length equal to the fin spacing, S_f. If the inlet conditions of the air and the liquid and vapour are known for one element, then the outlet conditions will be calculated by means of the mathematical model and the calculation procedure described in the previous section. Therefore, the calculation process must be started from the lowest element of the representative tube of the first row ($i = 1$, $j = 1$). For this element the inlet conditions of the air, liquid and vapour are known and the outlet conditions can be calculated. Hereafter, the elements of the tube can be solved from the bottom to the top ($i = 1, \ldots, n$, $j = 1$). Once the representative tube of the first row is solved, then the air conditions at the inlet of any incremental element in each tube of the second row are known and the tube elements can be solved from the bottom to the top ($i = 1, \ldots, n$, $j = 2$). Therefore, the representative tube for each consecutive row can also be solved one after another ($i = 1, \ldots, n$, $j = 3, \ldots, n_r$).

In each incremental element the heat and mass transfer processes should be considered simultaneously in order to obtain the outlet conditions, therefore the heat and mass transfer equations and mass, concentration and energy balances should be solved together. As shown in Eqs. (1) and (2), mass transfer depends on the value of the ratio z and the interface temperature. On the other hand, the heat transferred between the vapour and liquid phases given by Eqs. (6) and (7) depends on the interface temperature T_i and the ammonia and total mass transferred. Moreover, the heat flux transferred between the bulk liquid and the air, shown in Eqs. (10), depends on the outlet cooling air temperature T_{co}. Taking all these things into account, an iterative procedure must be implemented to solve Eqs. (1)–(23). The following algorithm uses three iterative loops to obtain the values of the ratio z, the interface temperature, T_i and the outlet cooling air temperature T_{co}. Once these parameters are calculated, the vapour and liquid conditions of the next incremental element can be obtained. The calculation procedure is summarised below.

(1) Guess the interface temperature, T_i.
(2) Calculate $\bar{x}_{Li}$ and $\bar{x}_{vi}$ with the assumed interface temperature and the absorber pressure, considering equilibrium and saturation conditions.
(3) Guess z.
(4) Calculate $\dot{n}_{NH_3}|_v$ and $\dot{n}_{NH_3}|_L$ from Eqs. (1) and (2).
(5) If $\dot{n}_{NH_3}|_v = \dot{n}_{NH_3}|_L$, go to step 6, otherwise guess a new value of z and go to step 4.
(6) Calculate the ammonia and total mass flux with Eqs. (4) and (5).
(7) Calculate the sensible heat transferred from vapour and liquid phases, using Eqs. (6), (7) and (8).
(8) Check the energy balance at the interface using Eq. (9). If verified, go to step 9, otherwise guess a new value of T_i and go to step 2.
(9) Guess T_{co}.
(10) Calculate the heat flux transferred from liquid to the air, using Eqs. (10), (11) and (12).
(11) Check T_{co} using Eq. (25). If the values are equal go to step 12, otherwise guess a new T_{co} and go to step 9.

$$T_{co} = T_{ci} + \frac{\varphi_c \cdot \Delta A_c}{\dot{M}_c \cdot c_{p,\text{air}}} \tag{25}$$

(12) The new vapour and liquid conditions can now be obtained from Eqs. (17)–(22).

The algorithm is applied as indicated previously at each incremental element from the bottom to the top of the tube and from the first row to the last one. The solution method explained above has been implemented in a computer program using FORTRAN 95. A more detailed discussion about the solution of this type of processes can be seen in Ref. [39]. State equations required for ammonia–water equilibrium and thermodynamic properties are taken from Ziegler and Trepp [40].

5. Results and discussion

The initial data required by the computer program are the absorber configuration and geometry, the material thermal properties and the operating conditions. The results provided by the program are the distributions along the tubes length of each row

Table 2
Geometry and material thermal properties of the absorber

Absorber length [m]	1.1
Inner tube diameter [m]	0.022
Outer tube diameter [m]	0.025
Fin spacing [m]	0.006
Fin thickness [m]	0.00045
Number of rows	4
Number of tubes	60
Transversal tube spacing [m]	0.05
Longitudinal tube spacing [m]	0.0433
Nozzle diameter [m]	0.009
Tube wall thermal conductivity [$W\,m^{-1}\,K^{-1}$]	13
Fin thermal conductivity [$W\,m^{-1}\,K^{-1}$]	204

Table 3
Absorber operating conditions

Vapour mass flow rate [$kg\,h^{-1}$]	15.0
Vapour concentration [(kg NH_3) kg^{-1}]	0.995
Vapour temperature [K]	288.15
Inner tube pressure [bar]	2.25
Weak solution mass flow rate [$kg\,h^{-1}$]	135.0
Weak solution concentration [(kg NH_3) kg^{-1}]	0.235
Weak solution temperature [K]	323.15
Cooling air-facing velocity [$m\,s^{-1}$]	2.5
Cooling air inlet temperature [K]	303.15

Table 4
Results

Row	1	2	3	4
Strong solution mass flow rate [$kg\,h^{-1}$]	37.5	37.5	37.5	37.5
Strong solution concentration [(kg NH_3) kg^{-1}]	0.310	0.310	0.310	0.310
Strong solution temperature [K]	307.38	307.88	308.37	308.89
Absorption length [m]	0.936	0.978	1.026	1.068

of several parameters such as: temperature, concentration and mass flow of the vapour and liquid phases, interface temperature and interface liquid and vapour concentrations, the tube wall and air temperatures; the ammonia, water and total molar fluxes transferred between phases, the ratio z of ammonia to total molar flux, the void fraction, the heat and mass transfer coefficients, the specific interfacial area, the fins efficiency and the heat transfer fluxes.

A representative absorber design and nominal operating conditions for a small capacity ammonia–water absorption refrigeration system were chosen to demonstrate the results obtained from the program and model described above [41]. Furthermore, a parametric study was carried out in order to analyse the influence of each design parameter and operating condition on the absorber performance. The noteworthy results that have an effect on the practical design of the absorber are presented and commented.

The specific configuration, geometry and material thermal properties of the absorber considered in the analysis are specified in Table 2. The nominal operating conditions are shown in Table 3. Direct numerical results from the program run are shown in Table 4. The detailed analysis of the temperature and concentration distributions of the liquid and vapour phases es-

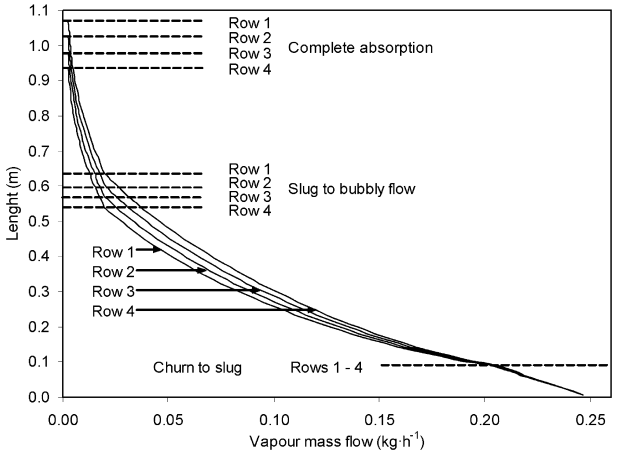

Fig. 4. Vapour mass flow rate profile along the length of the absorber tubes for each row.

tablished inside the tubes is reported and validated in Ref. [10] taking into account the data at disposal in the literature [42–46], therefore it is not repeated here. The results shown hereafter are concentrated on the particularities introduced by the air cooling of the absorber and those results that do not bring a new contribution to the results shown in Ref. [10] are omitted.

Fig. 4 shows the vapour mass flow rate along the length of the absorber tubes for each row. The horizontal dashed lines on the figure point out the transition between flow patterns (churn to slug and slug to bubbly flows) and the absorption achievement for the tubes of each row. It can be seen that the evolution of the absorption process is similar for the tubes in the four rows and the three different flow patterns are distinguished. The greatest part of the absorption process occurs in the slug flow regime as reported in [47] from the analysis of experimental data. Results of the vapour mass flow profile in the tubes also coincide with those in Ref. [10] and with the profiles obtained from experimental data reported in [19] for the mixtures NH_3–$LiNO_3$ and NH_3–NaSCN. However, it is clearly seen that the absorption process evolves more slowly from the first to the last row according to the air flow direction and consequently the length of the tubes required to complete the absorption process increases from the first to the last row (see results in Table 4). The different evolutions of the absorption process among the tubes of different rows are due to the air temperature increase when it moves through the tube rows in the bundle. The tube length from the bottom to the point where the absorption process is completed is named as the absorption length. Therefore, taking into account the results in Fig. 4 it is concluded that the absorption length is different for the tubes located in different rows and increases from the first to the last row according to the air flow direction. Then, the absorber design should be based on the absorption length of the last tube row.

Fig. 5 depicts the liquid phase temperature profiles along the tubes length in each row and the air temperature profiles along the tubes length at the outlet of each row. The liquid phase and the air temperature profiles result from the heat and mass transfer processes that take place inside the tubes and the heat

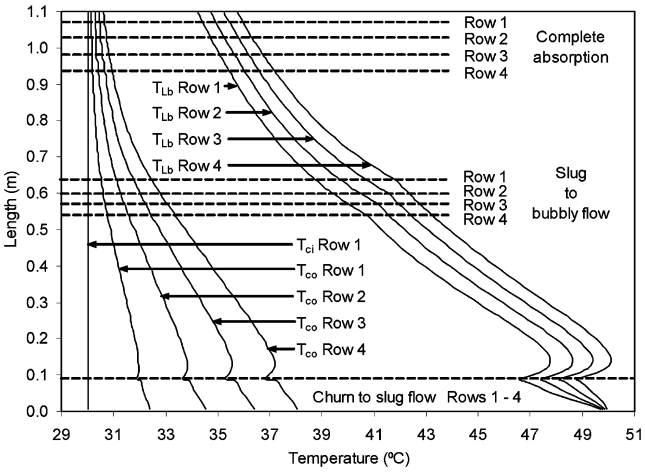

Fig. 5. Liquid phase temperature profile along the tubes length in each row and air temperature profiles along the tubes length at the outlet of each row.

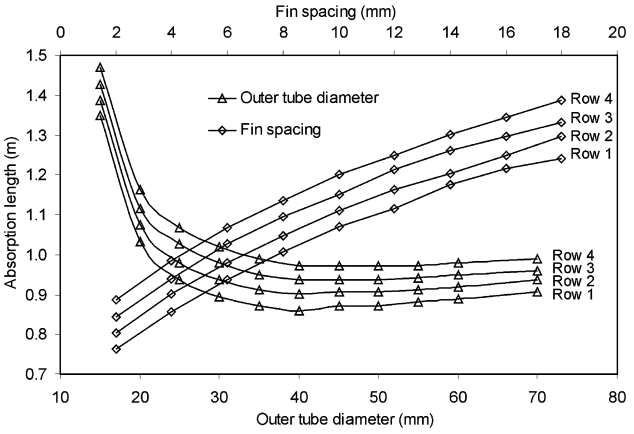

Fig. 6. Influence of the outer tube diameter and the fin spacing on the absorption length for each one of the tube rows.

transfer process from the liquid phase to the cooling air through the tubes wall and the fins. It can be seen that both temperature distributions are analogous. Both temperatures decrease from the bottom up to the end of the churn flow region. The slight temperature increase observed at the beginning of the slug flow region is due to the high mass and heat transfer rates at this absorption stage inside the tubes. Further, along the length of the tubes both temperatures drop continuously up to the top of the tubes. The air flow through the tube rows causes the inlet air temperature at each row to increase from the first to the last row of the tube bank according to the air flow direction. Therefore, the heat transfer from the two phase flow inside the tubes to the air is reduced and consequently it affects the absorption process taking place inside the tubes. Moreover, the continuous plate fins considered in the analysis prevent the air from mixing in the tubes direction. Therefore, the heating up of the air is different along the length of the absorber. It is clearly reflected in the air temperature profiles shown in Fig. 5 that the air temperature differences at the bottom of the absorber are much higher than the temperature differences at the top.

Parametric analysis was carried out in order to evaluate the influence of the geometrical design parameters and the operating conditions on the absorber design and performance. Each parameter was varied while keeping all other constant and equal to the data given in Tables 2 and 3. The effect of each parameter was evaluated by considering its influence on the tubes length required for the complete absorption achievement (absorption length).

The effect of the outer tubes diameter on the required absorption length for each one of the four tube rows is illustrated in Fig. 6. The four graphs in the figure correspond to the four tube rows of the absorber. It can be seen that the effect of the tubes diameter on the absorption length is similar for the four rows. The differences in the absorption length among rows remain nearly constant for each tube diameter. The influence of the tubes diameter agree with the conclusions given by Ferreira et al. [47] from the analysis of experimental data and with the results shown in Ref. [10] which state the existence of an optimum tube diameter that minimises the absorption length, the sharp impact of small tubes diameter (less than 25 mm) on the absorption length, as well as the small influence of the tube diameters greater than the optimum one. In this case, the optimum diameter changes slightly for each row. The diameter and length of the tubes are the key parameters from the standpoint of the absorber design. Therefore, the results presented in Fig. 6 can be very helpful and should be taken into account in order to decide the diameter and length of the tubes to build an absorber.

Fig. 6 also shows the influence of fin spacing on the absorption length for each one of the tube rows. Results reflect that the absorption length increases significantly when the fin spacing increases and this effect is similar for the four tube rows. It states clearly that this parameter plays an important role on the absorber sizing. Results in Fig. 6 allow concluding that the fin spacing should be reduced to a minimum. However, from a practical point of view, the fin spacing is limited by the available manufacturing technology. The main difficulties for reducing the fin spacing in this type of absorbers would be related with the use of steel or stainless steel tubes of a large diameter (see Fig. 6) and with attaining a good contact between the fins and tubes due to the complexity of mechanically expanding the tubes and therefore it would require a galvanised process. Fin spacing could be reduced to 4 or 6 mm.

Fig. 7 shows the influence of the cooling air temperature and the air-facing velocity on the absorption length for different tube rows. Results in Fig. 7 reveal the significant influence of these parameters on the absorber performance. The absorption length increases when the air temperature increases. This effect becomes more important for air temperatures higher than 30 °C. The air temperature increase influences slightly the differences in the absorption length among the different tube rows. The air velocity also has an important effect on the absorption length. The absorption length increases when the air velocity decreases and, in this case, this effect is stressed for low air velocities. These results agree with the experimental data reported in [42] when considered different coolant flow rates. Moreover, results in Fig. 7 show that the air velocity decrease also increases the differences in absorption length among the tube rows. Results in Fig. 7 should be taken into account to select the fan for the absorber.

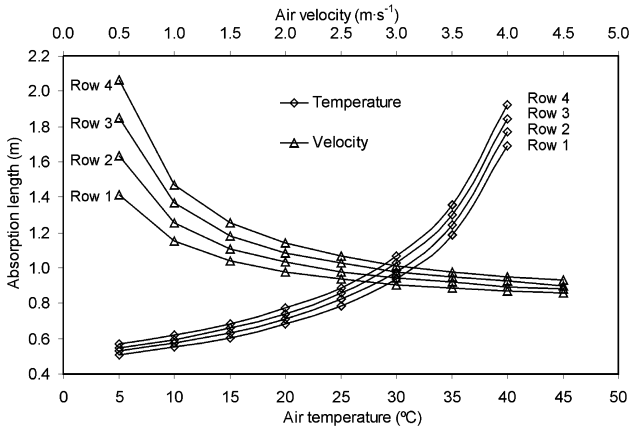

Fig. 7. Influence of the cooling air temperature and the air-facing velocity on the absorption length for each one of the tube rows.

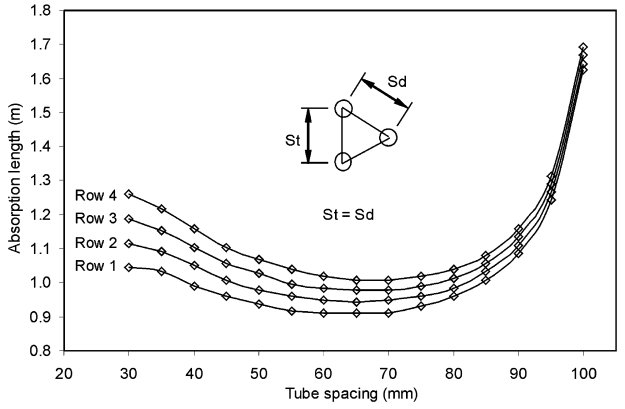

Fig. 8. The effect of the pitch between tubes for an equilateral staggered arrangement in the tube bundle.

Fig. 8 shows the effect of the pitch between tubes for an equilateral staggered arrangement in the tube bundle. Results reveal the existence of an optimum value for the pitch that minimises the absorption length. It is due to the effects of pitch on the finned surface, the air mass flow and the air velocity within the tube bank. On the one hand, the increase of the pitch enlarges the finned surface and increases the air mass flow, taking into account that the air-facing velocity to the absorber is considered constant; meanwhile, on the other hand, it reduces the air velocity inside the tube bank and consequently the air side convection coefficient. Generally, the optimum tubes pitch is different for each row. However, results in Fig. 8 show that the optimum values are close (between 65 and 70 mm) for the four rows. It is also noteworthy that high pitch values cause a significant increase of the absorption length, whereas pitch values lower than the optimum one increase the absorption length and the absorption length differences between the tubes in different rows.

Fig. 9 shows the influence of the tube bundle arrangement on the absorption length. The distribution of 60 tubes in bundles with different number of rows is considered and the absorption length corresponding to the last row of each bundle is represented. Results in Fig. 9 state clearly the influence of the tubes arrangement on the absorption length and therefore on the absorber sizing. It is mainly due to the air heating as it moves over the tube rows of the bank. Therefore, it is concluded that the tubes should be arranged with the less number of rows possible to avoid the detrimental effect of air heating at the first tube rows.

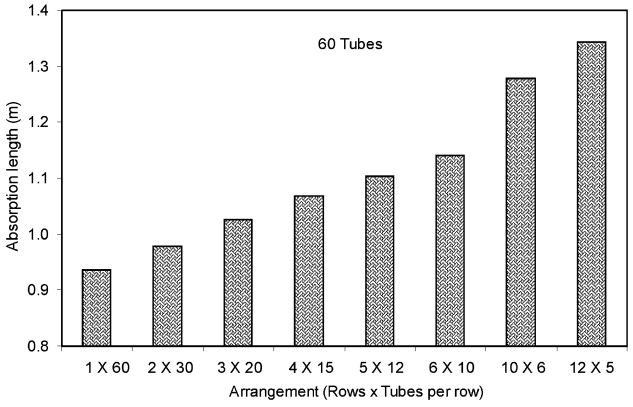

Fig. 9. Influence of the tube bundle arrangement on the absorption length.

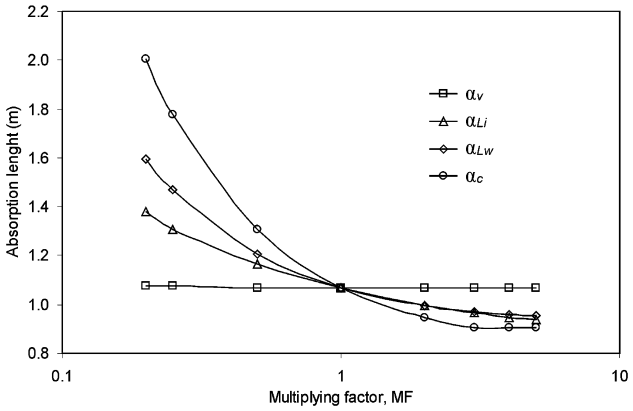

Fig. 10. The effect of heat transfer coefficients on the absorption length.

Fig. 10 shows the influence of the heat transfer coefficients in the liquid (α_{Li}) and vapour (α_v) phases, between the liquid and the tube wall (α_{Lw}) and in the air (α_c), on the highest absorption length which corresponds with the length of the tubes at the last row. Results in Fig. 10 clearly indicate that the heat transfer coefficient in the air side (α_c) has the most significant effect on the absorption process. The heat transfer coefficient between the liquid and the tube wall (α_{Lw}) is the next more important factor, followed by the heat transfer coefficient in the liquid–vapour interface (α_{Li}). These results also reflect that the heat transfer coefficient in the vapour phase has a negligible effect on the absorption process in this type of equipment.

6. Conclusions

In this paper, a detailed analysis of an ammonia–water vertical tubular absorber cooled by air has been presented. The analysis has been realised by means of a mathematical model based on mass and energy balances and the heat and mass transfer equations and taking into account separately churn, slug and bubbly flow patterns in the absorption process. The conclusions presented hereafter are a follow up to the conclusions

of Ref. [10], therefore only new contributions related to the air cooling of the absorber are reported.

The results show that the absorption process evolves more slowly from the first to the last tube row according to the air flow direction and consequently the length of the tubes required to complete the absorption of the ammonia into water is different for each row and increases from the first row to the last one. Therefore, the sizing of the absorber should be based on the absorption length required at the last tube row. Moreover, the results make clear that the arrangement of the tubes in the bundle has significant effect on absorption length and allow concluding that the tubes should be arranged with the less number of rows possible to avoid the detrimental effect of air heating at the first tube rows. If an equilateral staggered arrangement is used, then the existence of an optimum value for the pitch that minimises the absorption length can be established. It is also noteworthy that high pitch values cause a significant increase of the absorption length.

The results in this paper corroborate the existence of an optimum tube diameter that minimises the absorption length, the sharp impact that small tubes diameters have on the absorption length, as well as the minor influence of tube diameters greater than the optimum one. In the air-cooled absorber the optimum diameter changes slightly for each row. The fin spacing plays an important role on the absorber sizing and it should be reduced as much as possible, taking into account the limit imposed by the available manufacturing technology.

The air temperature profiles along the tubes length reflect that the heating up of the air increases from the bottom to the top of the absorber being more important at the bottom for the churn flow and at the beginning of the slug flow where high mass and heat transfer rates take place. The influence of the cooling air temperature and the air-facing velocity on the absorber performance is significant. The absorption length augments when the air temperature increases and it is stressed for air temperatures higher than 30 °C. The absorption length increases when the air velocity decreases and this effect becomes important for low air velocities. Moreover, the differences in the absorption length among the tube rows rise when the air velocity decreases. These results should be taken into account to select the fans for the absorber.

References

[1] J. Bassols, B. Kuckelkorn, J. Langreck, R. Schneider, H. Veelken, Trigeneration in the food industry, Appl. Therm. Engrg. 22 (2002) 595–602.

[2] P. Colonna, S. Gabrielli, Industrial trigeneration using ammonia–water absorption refrigeration systems (AAR), Appl. Therm. Engrg. 23 (2003) 381–396.

[3] D.S. Kim, C.H.M. Machielsen, Evaluation of air-cooled solar absorption cooling systems, in: R. Wang, Z. Lu, W. Wang, X. Huang (Eds.), Proceedings of the International Sorption Heat Pump Conference (ISHPC2002), Science Press, Shanghai, China, 2002, pp. 117–123.

[4] M. Medrano, M. Bourouis, A. Coronas, Absorption of water vapour in the falling film of water–lithium bromide inside a vertical tube at air-cooling thermal conditions, Int. J. Therm. Sci. 41 (2002) 891–898.

[5] J. Castro, P. Pozo, L. Leal, A. Oliva, Operation analysis of a laboratory prototype of an air-cooled absorption refrigerating machine with H_2O–LiBr as working fluid, in: J. Fernández-Seara, M. Vázquez (Eds.), Avances en ciencias y técnicas del frío II, Vigo, Spain, 2003, pp. 260–269.

[6] M. Ogawa, T. Yoshida, Y. Oda, Study on heat transfer analysis for the vertical condenser/absorber of an air-cooling absorption chiller/heater, in: Proceedings of the Absorption Heat Pump Conference '91, Japan, 1991, pp. 225–230.

[7] J. Fernández-Seara, M. Vázquez, Study and control of the optimal generation temperature in NH_3–H_2O absorption refrigeration systems, Appl. Therm. Engrg. 21 (2001) 343–357.

[8] R.M. Lazzarin, A. Gasparella, P. Romagnoni, Experimental report on the reliability of ammonia–water absorption chillers, Int. J. Refrig. 19 (1996) 247–256.

[9] I. Horuz, T.M.S. Callander, Experimental investigation of a vapour absorption refrigeration system, Int. J. Refrig. 27 (2004) 10–16.

[10] J. Fernández-Seara, J. Sieres, C. Rodríguez, M. Vázquez, Ammonia–water absorption in vertical tubular absorbers, Int. J. Therm. Sci. 44 (2005) 277–288.

[11] W.K. Lewis, W.G. Whitman, Principles of gas absorption, Ind. Engrg. Chem. 16 (1924) 1215–1220.

[12] R.B. Bird, W.E. Steward, E.N. Lightfoot, Transport Phenomena, Wiley, New York, 1960.

[13] R.E. Treybal, Mass Transfer Operations, McGraw-Hill, New York, 1980.

[14] D.R. Webb, The condensation of vapour mixtures, in: Heat Exchanger Design Handbook, Begell House, 1998.

[15] T.K. Sherwood, R.L. Pigford, C.R. Wilke, Mass Transfer, McGraw-Hill, New York, 1975.

[16] T.E. Schmidt, Heat transfer calculation for extended surfaces, Refrigerating Engineering 57 (1949) 351–357.

[17] K.T. Hong, R.L. Webb, Calculation of fin efficiency for wet and dry fins, HVAC&R Research 2, (1996) 27–41.

[18] T. Perrotin, D. Clodic, Fin efficiency calculation in enhanced fin-and-tube heat exchangers in dry conditions, in: Proceedings of the 21st International Congress of Refrigeration, Paper No. ICR0026, 2003.

[19] C.A. Infante Ferreira, Vertical tubular absorbers for ammonia–salt absorption refrigeration, PhD thesis, Delft University of Technology, The Netherlands, 1985.

[20] T. Ueda, On upward flow of gas–liquid mixtures in vertical tubes (2nd report, consideration of frictional pressure drop and void fraction), Bulletin of JSME 10 (1967) 1000–1007.

[21] H. Hikita, K. Ishimi, Frictional pressure drop for laminar gas streams in wetted-wall columns with co-current and counter-current gas–liquid flow, J. Chem. Engrg. Jpn. 9 (1976) 357–362.

[22] P. Griffith, G.B. Wallis, Two-phase slug flow, ASME J. Heat Transfer 83 (1961) 307–320.

[23] G.F. Hewitt, Gas–liquid flow, in: Heat Exchanger Design Handbook, Begell House, 1998.

[24] D.J. Nicklin, J.O. Wilkes, J.F. Davidson, Two-phase flow in vertical tubes, Trans. Inst. Chem. Engrg. 40 (1962) 61–68.

[25] N. Zuber, J.A. Findlay, Average volumetric concentration in two-phase flow systems, Trans. ASME J. Heat Transfer 87 (1965) 453–468.

[26] H.S. Hikita, K. Tanigawa, K. Segawa, M. Kitao, Gas hold-up in bubble column, Chem. Engrg. J. 20 (1980) 59–65.

[27] T.H. Chilton, A.P. Colburn, Mass transfer (absorption) coefficients, Ind. Engrg. Chem. 26 (1934) 1183–1187.

[28] V. Gnielinski, New equations for heat and mass transfer in turbulent pipe and channel flow, Int. Chem. Engrg. 15 (1976) 356–368.

[29] R. Clift, J.R. Grace, M.E. Weber, Bubbles, Drops and Particles, Academic Press, New York, 1978.

[30] W. Nusselt, Die oberflachenkondensation des wasserdampfes, Z. Ver. Deut. Ing. 60 (1916) 541.

[31] S.S. Kutateladze, Fundamentals of Heat Transfer, Academic Press, New York, 1963.

[32] J.M. McNaught, D. Butterworth, Film condensation of pure vapour, in: Heat Exchanger Design Handbook, Begell House, 1998.

[33] A.P. Lamourelle, O.C. Sandall, Gas absorption into a turbulent liquid, Chem. Engrg. Sci. 27 (1972) 1035–1043.

[34] G.A. Hughmark, Holdup and mass transfer in bubble columns, Ind. Engrg. Chem. Proc. Des. Dev. 6 (1967) 218–220.

[35] W.D. Deckwer, On the mechanism of heat transfer in bubble column reactors, Chem. Engrg. Sci. 35 (1980) 1341–1349.

[36] W.M. Kays, M.E. Crawford, Convective Heat and Mass Transfer, McGraw-Hill, New York, 1980.
[37] C. Keizer, Absorption refrigeration machines, PhD thesis, Delft University of Technology, The Netherlands, 1982.
[38] F.C. McQuiston, J.P. Parker, Heating, Ventilating and Air-Conditioning. Analysis and Design, John Wiley & Sons, New York, 1994.
[39] J. Sieres, J. Fernández-Seara, F.J. Uhía, M. Vázquez, Solution of the simultaneous heat and mass transfer equations in ammonia–water absorption system process, in: J.P. Meyer, A.G. Malan (Eds.), Proceedings of the Fourth International Conference on Heat Transfer, Fluid Mechanics & Thermodynamics (HEFAT 2005), Cairo, Egypt, 2005.
[40] B. Ziegler, Ch. Trepp, Equation of state of ammonia–water mixtures, Int. J. Refrig. 7 (1984) 101–106.
[41] J. Fernández-Seara, J. Sieres, M. Vázquez, Absorption refrigeration prototype for on board cooling production in fishing vessels, in: R. Wang, Z. Lu, W. Wang, X. Huang (Eds.), Proceedings of the International Sorption Heat Pump Conference (ISHPC2002), Science Press, Shanghai, China, 2002, pp. 130–135.
[42] H.Y. Kim, B.B. Saha, S. Koyama, Development of a slug flow absorber working with ammonia–water mixture: Part I—Flow characterization and experimental investigation, Int. J. Refrig. 26 (2003) 508–515.
[43] H.Y. Kim, B.B. Saha, S. Koyama, Development of a slug flow absorber working with ammonia–water mixture: Part II—Data reduction model for local heat and mass transfer characterization, Int. J. Refrig. 26 (2003) 698–706.
[44] Y.T. Kang, R.N. Christensen, T. Kashiwagi, Ammonia–water bubble absorber with a plate heat exchanger, ASHRAE Trans. 104 (1998) 956–966.
[45] Y.T. Kang, A. Akisawa, T. Kashiwagi, Analytical investigation of two different absorption modes: falling film and bubble types, Int. J. Refrig. 23 (2000) 430–443.
[46] G.S. Herbine, H. Pérez-Blanco, Model of an ammonia–water bubble absorber, ASHRAE Technical Data Bulletin 11 (1995) 102–110.
[47] C.A.I. Ferreira, C. Keizer, C. Machielsen, Heat and mass transfer in vertical tubular absorbers for ammonia–water absorption refrigeration systems, Int. J. Refrig. 7 (1987) 348–357.